International Journal of Innovative Computing, Information and Control
Volume **8**, Number **10(B)**, October **2012**

ICIC International ©2012 ISSN 1349-4198
pp. 6999–7016

SENSOR MODELING FOR PORTABLE ELECTRICAL CAPACITANCE TOMOGRAPHY SYSTEM USING SIMULATION BY COMSOL MULTIPHYSICS

Elmy Johana Mohamad[1], Muhammad Afiq Zimam Mohamed[2]
Ruzairi Abdul Rahim[2], Leow Pei Ling[2], Mohd. Hafiz Fazalul Rahiman[3]
Khairul Hamimah Abas[2] and Salinda Bunyamin[2]

[1]Department of Mechatronics and Robotics Engineering
Faculty of Electrical Electronics Engineering
Universiti Tun Hussein Onn Malaysia
Pt. Raja, Bt. Pahat, Johor 86400, Malaysia
elmy@uthm.edu.my

[2]Process Tomography and Instrumentation Research Group, Cybernetics Research Alliance
Faculty of Electrical Engineering
Universiti Teknologi Malaysia
UTM Skudai, Johor 81310, Malaysia
zimam_88@yahoo.com; { ruzairi; leowpl }@fke.utm.my

[3]School of Mechatronic Engineering
Universiti Malaysia Perlis
Arau, Perlis 02600, Malaysia
hafiz@unimap.edu.my

Received June 2011; revised October 2011

Abstract. *This work presents the development process for modeling a 16-segmented portable ECT (Electrical Capacitance Tomography) sensor (using FEM software package COMSOL Multiphysics). The physical sensors are 3D dimensional but it has been common to model the slice or the cross-section in 2D. This project shows the modeling approach for 2D and 3D geometries, the linear Finite Element method (FEM) using COMSOL Multiphysics is developed in order to obtain the capacitance between electrodes when an electric field is applied and to obtain the permittivity distribution inside the closed pipe from the sensor. Generated phantoms and measured values are presented for empty and annular pattern. The sensor model will be used to simulate a real sensor. Simulation is verified using phantoms with different sizes and at different locations inside the 16 electrode sensor space. Simulation and initial experimental results illustrate the capability of the system presented. Result due to increasing the size of permittivity of the dielectric material and their effect on the reconstructed image in Electrical Capacitance Tomography system are also discussed. The ECT model is representative by existing hardware, portable ECT, PROTOM Research Group UTM, Malaysia.*
Keywords: Portable, Electrical capacitance tomography, Process tomography, Sensor modeling, COMSOL multiphysic

1. **Introduction.** An ECT system is able to obtain information about the contents of vessels, based on measuring variations in the dielectric properties of the flowing material inside the vessel. ECT can be used with vessels of any cross-section, but most work to-date has used circular geometries [1]. A typical ECT system consists of a sensor built up from 8, 12 or 16 electrodes, capacitance measurement circuit, central control unit and a control PC [2]. The electrode which is normally built from conductive plate acts as sensing surface that directly contacts to the measuring area. The capacitance measuring circuit or better

known as signal conditioning circuit is used to collect data and convert the measurement readings to digital. A central control unit is designed to synchronize all the operations and transfer the data to a control PC. A control PC that receives the measurements reading will store the acquired data, reconstruct images from the integral measurements and take action feedback to control the flow [3]. These works are concentrated on designing ECT modeling system with portable and mobile ability, and thus external electrodes must be chosen instead of internal electrodes. A sixteen segmented sensor electrodes were developed in this work which mounted symmetrically on the outer surface of an insulating vertical pipeline.

An ideal capacitance measuring system will have a very low noise level, a wide dynamic measurement range and high immunity to stray capacitance. Stray capacitance is a type of noises where the leakage capacitance is due to connection from the circuit and cable to the electrode [1]. In a practical ECT system, there are three main sources of stray capacitance which affect the capacitance measurement: screened cable, CMOS switches and sensor screen. A 1m long screened cable connecting the sensing electrode to the measuring circuit introduced, is about 100pF of stray capacitance [4]. Additionally the stray capacitance may vary with cable movement, ambient temperature changes, component variation and external or internal electric field changes [5]. Typical capacitance values are in a range between 0.5 and 0.01pF. Consider that the measurement error should be better than 1% for all capacitance measurements [6].

In most of previous researches regarding ECT, the signals from the sensor electrodes are usually connected to the signal conditioning circuit by using coaxial cable. The coaxial cable is able to shield disturbance or stray capacitance and thus introduce a very low noise solution. However, the cable connecting the measuring electrode and signal conditioning circuit introduces the most part of the stray capacitance. Therefore, the connecting cables should be made as short as possible. Thus in this project we proposed better solution by completely removing the use of cables to connect between the electrode plates and signal conditioning circuit, which can be termed as direct mounting technique. The signal conditioning circuit which is built on the electrode sensor becomes an ECT sensor module. This module not only reduces the noises, but also can work independently.

2. **Portable ECT Sensor Description.** The new approach of this portable ECT system is to allow suppleness of the system to be assembled and moved from a pipeline to another. The system is designed to be able to accommodate different diameter sizes of pipeline and flexibility of numbers of electrodes sensor usage depending on different size of pipeline without the need of redesigning the electrodes sensor. These sensors able to work independently [7].

Universal Serial Bus technology (USB) is used for the data transferring with the purpose of providing high data transfer rate to PC. A microcontroller work as the centralization control unit is used to support full-speed USB data transfer rate. The information obtained in the PC will be reconstructed using linear back projection (LBP) algorithm. There are difficulties with image reconstruction in ECT, the relationship between the permittivity distribution and capacitance is non-linear and the electric field is distorted by the presence of the material, called as 'soft-field' effect [4]. This leads to the use of linearized algorithm to relate the capacitance measurements to the pixel values in the image and vice-versa. The only image reconstruction algorithm which is fast enough to be used for in gas/water two-phase distribution on-line image display is the linear back projection method. This produces approximate images which are of acceptable quality for many applications. The method is based on linearization of a normalized form of the measured capacitance. Another method than having high-speed capabilities in on-line

image reconstruction is Calderon's method. These algorithms give quantitative results and one of the fastest methods for on-line image reconstruction. Nevertheless, the reconstruction algorithm is valid and effective for low contrast dielectrics such as oil and gas [8]. Other methods can be used to produce improved images off-line from captured capacitance measurements. These methods involve the use of iterative computational methods, or alternatively, the application of neural network techniques [9].

By using LBP method, it can be used to measure the flow rate and the concentration of material distribution through a pipelines, these techniques gives a better understanding of the flow through the regime and the data can be used to design better future process equipment which to control certain processes to optimized the production and monitoring the quality of any process. Figure 1 illustrates the topology of an ECT system where the ECT sensor consists of sixteen electrodes mounted equidistantly along the periphery of an insulated pipe vessel. The 16 segmented electrodes are numbered from 1 to 16, and the measurement protocol in the sensing electronics first measures the inter-electrode capacitance between electrodes one and two, then between one and three, and up to one and N, where $N = 16$ in this case. Then, the capacitances between electrodes two and three, and up to two and N are measured. The measurements continue until all the inter-electrode capacitances are measured.

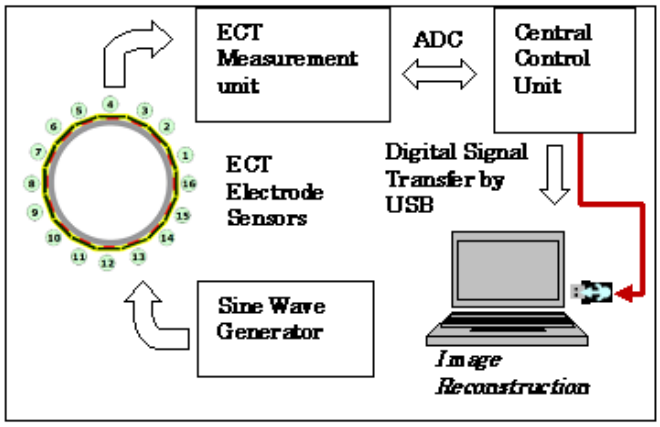

FIGURE 1. ECT system topology

3. **ECT Sensor Modeling.** To be able to analyze the ECT system and make optimal sensor design, it is preferable to have a mathematical model of the ECT sensor head. In this way, the effect of the numerous design parameters can be analyzed by simulations. The numerical techniques involved in image reconstruction also demand the use of a mathematical model of the sensor, even if some image-reconstruction techniques can be based purely on empirical data. It is difficult to calculate an inter-electrode capacitance which relate with the relative permittivity distribution $\varepsilon(r)$ and potential distribution $\varphi(r)$, by using the Laplace equation is still too difficult to solve for the geometry and the boundary conditions, thus a finite element method (FEM) software simulation package is need to be used to find the electric field distributions [10-12].

The creation of a capacitance sensor model in COMSOL aims to obtaining a method from which numerical calculation can be carried out for the electric potential (φ) in the space of the sensor [6]. The first step to develop the numerical modeling is by drawing the shape of a pipeline which is a circle with a certain diameter. For this case, the drawing geometry used will follow the hardware actual size and geometry. Then alteration of the number of electrodes around the pipeline can be easily built. The relationship between

the spatial distribution of the permittivity and the measured capacitances can be derived from Maxwell's equation as in (1). Gauss' Law expresses the dielectric flux density $D(r)$

$$\nabla.D(r) = \rho_v(r) \tag{1}$$

The $\rho_v(r)$ stands for the volume charge density, while ∇ is the divergence operator. In ECT, only one electrode be excited at a time and the rest always at virtual earth potential, this total electric flux over all the electrode surfaces can be calculated as zero, thus the volume charge density is also zero, given

$$D = \varepsilon(r)E(r) \tag{2}$$

$$E(r) = -\nabla\varphi(r) \tag{3}$$

With ∇ is the gradient operator so we have

$$D(r) = -\varepsilon(r)\nabla\varphi(r) \tag{4}$$

where $\varepsilon(r)$ is the spatial permittivity distribution, $E(r)$ is the electric field intensity and $\varphi(r)$ is the electrical potential distribution within the sensor. As in (4) into (1) giving Poisson's equation

$$\nabla.[\varepsilon(r)\nabla\varphi(r)] = 0 \tag{5}$$

For a two-dimensional case $r(x, y)$ thus gives $\varepsilon(x, y)$, is the relative permittivity distribution in two dimensions with the boundary conditions, where $\varphi = V_C$ for the fired electrode and $\varphi = 0$ for the remaining electrodes, the capacitance measured between a pair of electrodes is expressed by the following expression

$$C = \frac{Q}{V_c} - \frac{\oint_s \varepsilon(x, y)\nabla\varphi(x, y)ds}{V_c} \tag{6}$$

where V_C is the potential difference between the source and the detecting electrode, Q is the total charge and S is the close line. The sensor model will be used to simulate real sensor. This means it will be able to solve the ECT forward problem calculating capacitances between all possible electrode pairs. To achieve this, (5) has to be solved first and in this way the potential distribution $\varepsilon(x, y)$ is obtained within the sensor. A way to calculate $\varphi(x, y)$ is by using finite element method (FEM).

By using this method, an approximation to the potential φ will be obtained in the sensor at a finite set points corresponding to the nodes of the triangular mesh that normally used in finite element method. Once the potential distribution is found within the sensor, the electric charge, Q_{ij} on each detector is calculated by using Gauss's Law as in (7)

$$Q_j = \oint_{sj} (\varepsilon(x, y)\nabla\varphi(x, y).n)ds \tag{7}$$

S_j is a closed curve surrounding the detector electrode and n is the normal vector along S_j. The potential distribution calculation $\varphi(x, y)$ by means of FEM as well as the Q_{ij} solution in this work directly implemented with COMSOL Multiphysics. Finally, the capacitance can be computed by an energy method, the energy required to charge a capacitor is given by the expressions

$$W_e = \frac{Q^2}{2C} \tag{8}$$

which is equal to the energy of the electrostatic field. This is available in the electrostatics module of COMSOL Multiphysics. So the capacitance is easily obtained from

$$C = \frac{Q^2}{2W_e} \tag{9}$$

4. **Modeling Process Using COMSOL Multiphysics.** The design process for an ECT sensor model consists of the following steps; geometry generation according to dimensions to be simulated, boundary conditions assignment and assignment of physical conditions in sensor sub-domains or zones. The design process for 16 portable electrode sensor models can be divided into following approach:

a) Choosing the mode in the electrostatics module
b) Geometry modeling according to dimension to be simulated
c) Generating the mesh
d) Set electrical properties in the domains
e) Set the boundary conditions

The detail of the physical sensor can be found in Table 1.

TABLE 1. Physical sensor parameter

no	item	parameter
1	Num of electrode plate	16
2	Electrode length	100mm
3	Inner pipe diameter	100mm
	Outer pipe diameter	110mm
4	Permittivity of the dielectric	$\varepsilon_r = 80$ (water) $\varepsilon_r = 1$ (air) $\varepsilon_r = 3$ (oil)

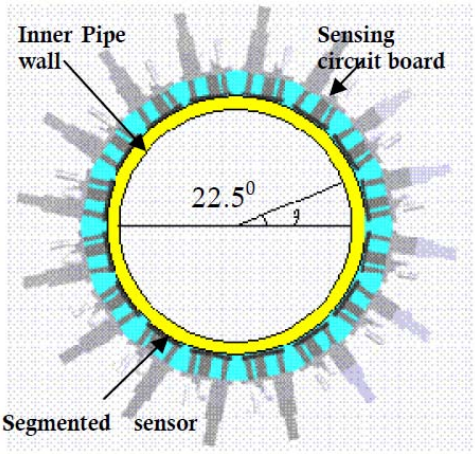

FIGURE 2. Illustration of sixteen sectors of portable ECT

Figure 2 shows an arrangement of 16 electrodes sensor on pipelines that has been designed in this project to cover 11cm acrylic pipe in diameter with wall thickness of 0.5cm, R_1 is inner pipeline radius 5cm, R_2 is outer pipeline radius, 5.5cm and electrode stretch angle θ is 22.5°.

4.1. **Preparing for simulations.** The modelling approach used in this study can be listed as:

a) Choosing the mode in the EM Module
b) Drawing the sensor geometries
c) Generating the mesh
d) Set electrical properties in the domains

e) Set the boundary conditions
f) Solve and find the field distribution
g) Use the post-processing capabilities in COMSOL to compute capacitance and voltage

The 2D and corresponding 3D geometries of the 16 segmented portable ECT are illustrated in Figure 3. The detail of the sensor can be found in Table 1.

4.2. **FEM meshing.** In this work, besides the insulating pipe, measurement electrodes, guard electrodes, the geometry includes the spatial discretization of the inner part of the sensor, a 32×32 square matrix has a number of 1024 pixels but only 830 pixels contribute to represent the image plane and another 194 pixels lie outside the pipe boundary. This diagram corresponds to the space within the R_1 radius in Figure 2. The meshes used to apply the FEM scheme. Figure 4 shows the finite element meshing in 2D of the portable ECT as appear in COMSOL Multiphysics. The meshing is performed with different parameters for each zone in order to get uniform definition in the area to be visualized and much higher definition near the electrodes, where need more accuracy.

4.3. **Set electrical properties domain and boundary condition.** After drawing the geometry of ECT, the next step is to assign the boundary and subdomain settings. Boundary conditions used are ground, port and distributed capacitance. On the other hand, the conditions for subdomain depend on the constant permittivity such as water, air and oil. The equations used for the boundary and subdomain conditions as follows:

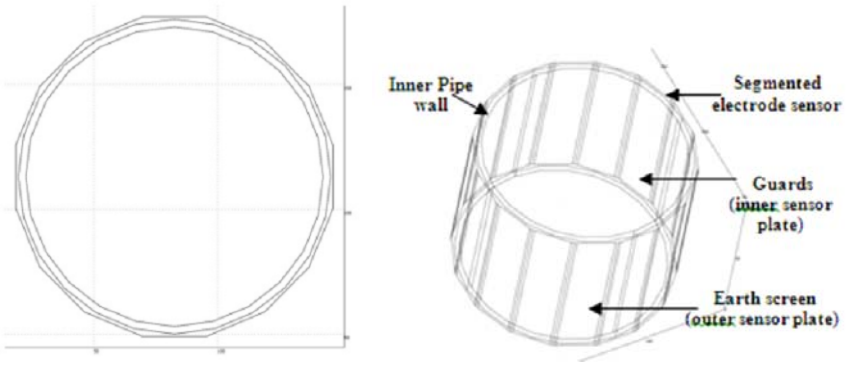

(a) (b)

FIGURE 3. (a) 2D segmented geometry of portable ECT sensor, (b) 3D geometry of portable ECT sensor

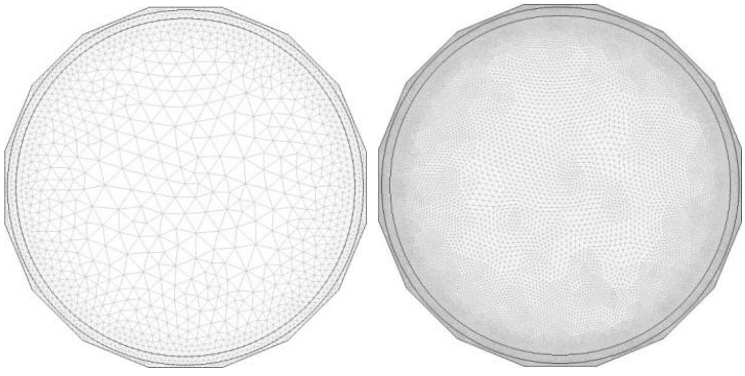

(a) (b)

FIGURE 4. FEM meshing: (a) initial mesh, (b) finer mesh

1) $n(D_1 - D_2) = \frac{\varepsilon_0 \varepsilon_r (V_{ref} - V)}{d}$, for distributed Capacitance.
2) $V = 0$, for ground.
3) $C = \frac{Q}{V}$, for port (excitation electrode).

The subdomain setting is

1) $-\nabla . d\varepsilon_0 \varepsilon_r \nabla V = d\rho$,

where
ε_0 is the relative permittivity,
ρ is the space charge density in C/m^3,
d is the thickness in mm.

4.4. **Preparing of excitation electrode.** ECT operates by reading the potential difference from the excited electrode to the detecting electrode. For example, when Electrode 1 is given voltage, the rest of the electrode will be the detecting electrode, the potential difference between inter-electrode capacitance will verified. The basic principles of ECT sensors have been described by many publications. In ECT, the object to be imaged is surrounded by electrodes, which act as both sources and detectors. The electrodes are excited one by one, or in pairs depending on the protocol used. At any point in time only one electrode or a pair of electrodes is excited, while the remaining electrodes function as detectors. The term protocol mainly refers to the sequence used to excite the sensor electrodes, and the order in which the signals are acquired.

For example, if Electrode 1 is made the source electrode, the rest electrodes function as detector electrodes. The detector electrodes are connected to the virtual ground terminals, so that they remain at zero potential with respect to ground. The capacitances between Electrode 1 and the others are measured. After measuring all the possible pairs of capacitances, Electrode 2 is made the source electrode and the measurement process is repeated. The whole cycle of exciting an electrode and measuring the resulting inter-electrode capacitances is repeated. The total number of electrode s given by N and the independent inter-electrode capacitance measurements M is given by

$$M = \frac{N(N-1)}{2} \tag{10}$$

Figure 5 showing a schematic representation of electric field lines that exist between any two electrodes are not straight. The field lines are curved instead.

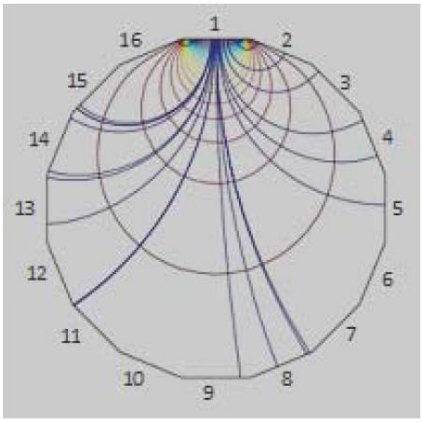

FIGURE 5. Number of electrodes on ECT

5. **Simulation Setup.** It is difficult to calculate an inter-electrode capacitance which relate with the relative permittivity distribution $\varepsilon(r)$ and potential distribution $\varphi(r)$, by using the Laplace equation is still too difficult to solve for the geometry and the boundary conditions, thus a finite element method (FEM) software simulation package is need to be used to find the electric field distributions. In this project the COMSOL Multiphysic is used to carry out the FEM simulation to find the electrical potential distribution in the space of the sensor. Therefore, we can relate the permittivity and potential difference by using

$$C = \frac{kA\varepsilon_o}{d} \tag{11}$$

where C = capacitance (F), ε_o = permittivity of dielectric (fluid flow), k = is the constant, A = area of the plate, d = the distance between those plates.

$$C = \frac{Q}{V_{1,2}} \tag{12}$$

where Q is the charge of the two conductors, $V_{1,2}$ is the voltage difference between the two conductors.

Note that Equation (11) and Equation (12) can be used to measure the capacitance of a certain material flow in a pipeline. For the ECT, to solve Equation (5), the Electrostatic solver is used, at it has after we set the boundary condition and subdomain setup, as it has better performance for solving such as Laplace and Poisson. Finally, capacitance calculation is performed between the models electrode-pairs by means of the method describe in Section 3. Figure 6 shows an example when Electrode 1 is charged (excitation electrode), in that moment measurements (simulated) are taken between it and the other 15 electrodes (grounded electrodes). The same occurs with all electrodes to make a total, $M = 120$ measurements.

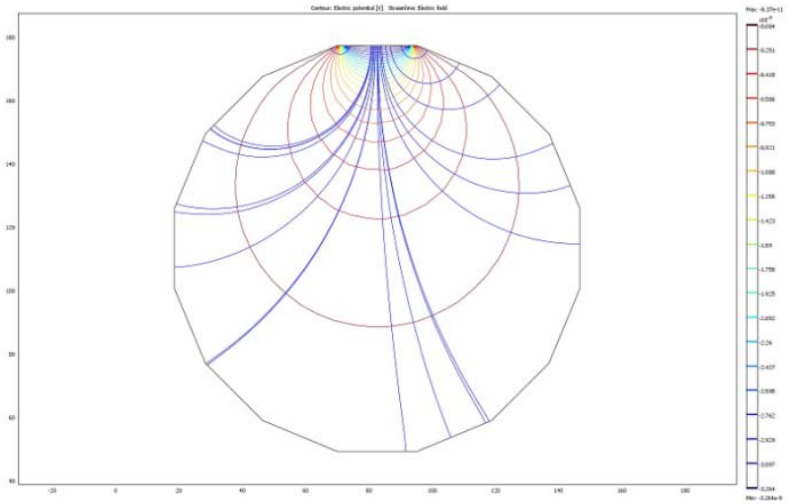

FIGURE 6. Electrical filed and potential lines for single excited electrode

5.1. **Single excitation electrode for 16 sensors.** To verify simulation, an annular phantom was created. The phantom used in this cases is as illustrated in 2D case, where a 20mm in diameter is located with its right at coordinates $x = 60$mm and $y = 125$mm, The permittivity distribution in this case is water, with relative permittivity $\varepsilon_r = 80$. The electrical field distribution for 2D simulation, when Electrode 1 is excited, is illustrated in Figure 7.

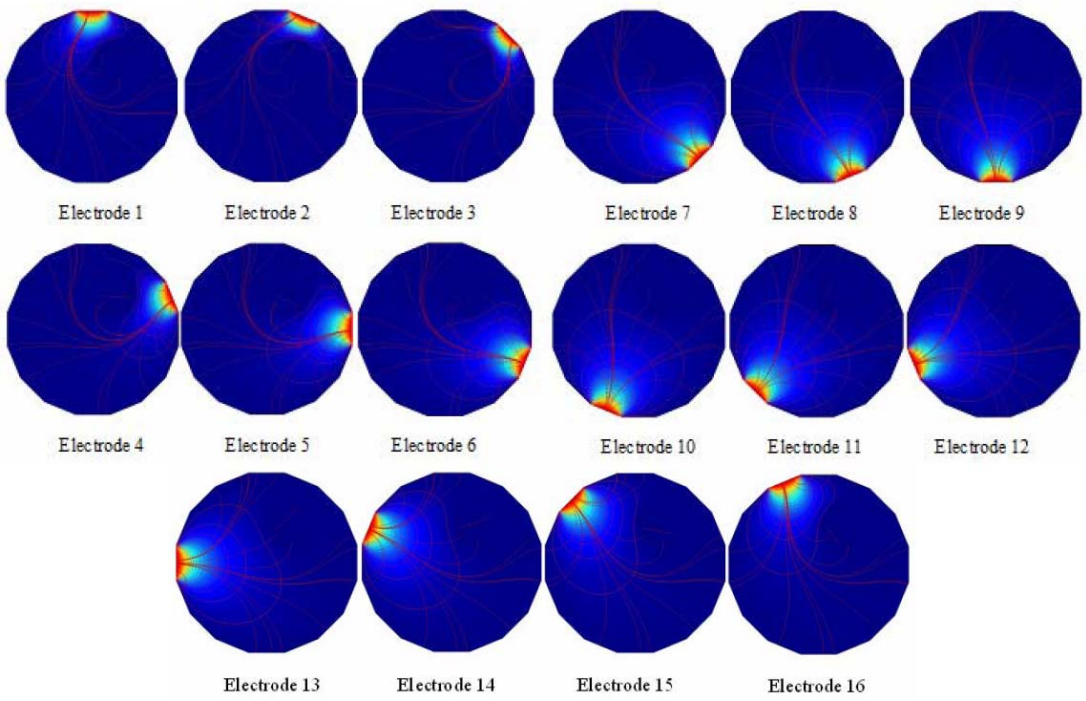

FIGURE 7. Potential distribution and image reconstructed

6. **Simulation Model Result.** Model results can be evaluated by comparing for the permittivity phantoms, empty (air permittivity = 1) against full with water, and all follows simulation was verified:

a) Image reconstructed for 2D when Electrode 1 is excited.
b) Electrical field lines for 3D simulation when Electrode 1 is excited.
c) Image reconstructed for 2D when all electrode is excited.
d) The effect of increasing the size of permittivity.
e) Image reconstructed simulation with different mixture of permittivity.

6.1. **Potential difference versus number of electrodes.** Two sets of potential difference are calculated by subtracting the potential at the area without water from the potential at the area with water as a phantom. The potential difference has larger values when there is water as the permittivity because the voltage loss exists is larger compared when without water. Figure 8 shows the potential distribution.

6.2. **Permitivity distribution.** The permittivity distribution in the simulations was verified. The 2D corresponding 3D geometries the ECT is illustrated in Figure 9. The Capacitance is performed between the model electrode-pairs and the electrical field distribution for 2D and 3D simulation, when Electrode 1 is excited, are illustrated in Figure 9 and all electrodes excited is in Figure 10. The phantom used as illustrated in the 2D where a 50mm in diameter, cylindrical phantom of water surrounded by air, is located with its centre at coordinates $x = 70$ and $y = 130$. As can be seen, the electrical field lines are deflected, depending on material distribution.

6.3. **The effect of increasing the size of permittivity.** Taking the annular phantom into consideration, the effect of increasing the size of permittivity is analyzed to find out how this effect the capacitance measurement and image reconstructed. The image sequences of increasing of diameter of dielectric are shown in Figure 10. Electrical field lines tend to follow the shape of the phantom with the increase size of permittivity.

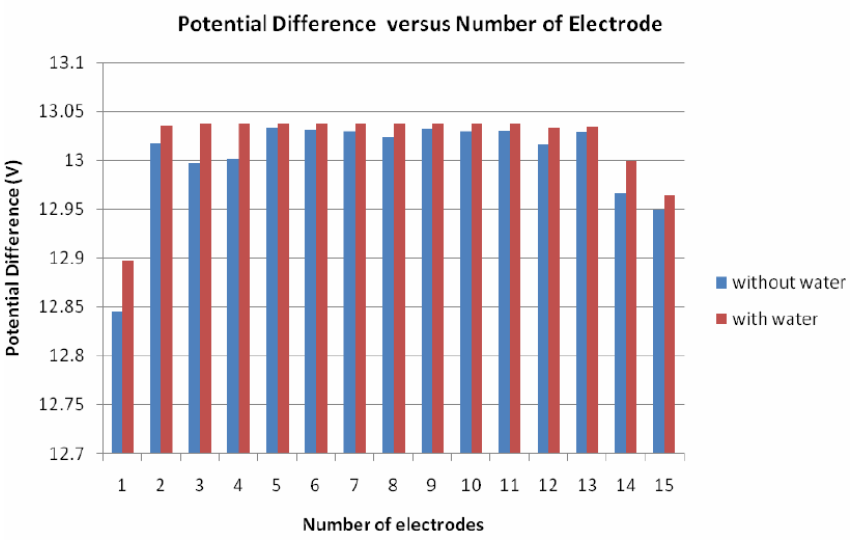

FIGURE 8. Potential differences with water and without water

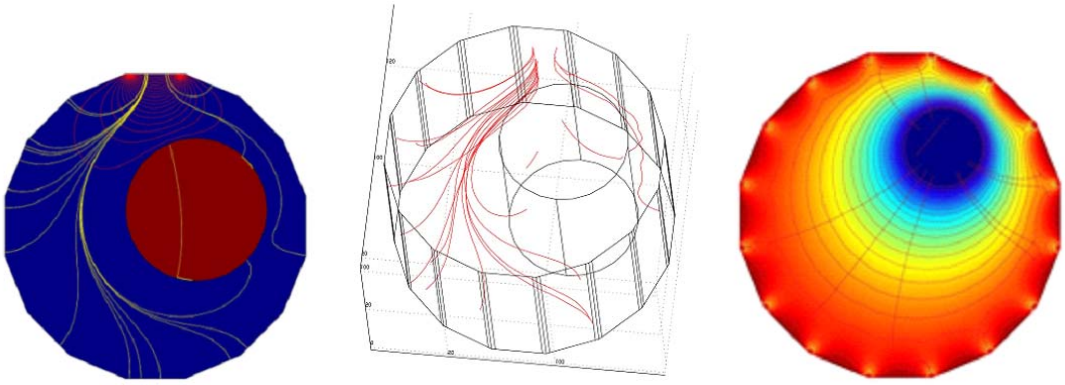

(a) (b) (c)

FIGURE 9. Results from (a) 2D and (b) 3D simulation, respectively. Blue area is sensing region represent air ($\varepsilon_{\text{air}} = 1$), and red area represents water ($\varepsilon_{\text{water}} = 80$) while (c) electrical field distributions for 2D when all electrodes were excited.

The data collected in Figure 11, shows non linearity of the standing capacitance changes due to the increasing of the size permittivity material. For a sensor with internal electrodes, the components of capacitance due to the electrical field inside the sensor will always increase in proportion to the material permittivity when the sensor is filled with higher uniformly with higher permittivity material. However, for the sensor with external electrodes, the permittivity of the wall causes non-linear changes in capacitance which may increase or decrease depending on the wall thickness and the permittivity's of the sensor wall and contents.

6.4. **Different mixture of permittivity.** Figure 12 below shows that the degree of penetration of electrical field depends on the permittivity of the material. The permittivity of material; $\varepsilon_{\text{water}}$ is 80, ε_{air} is 1 and ε_{oil} is 3.25, water has the highest permittivity and air has the lowest permittivity thus the electrical fields seem to be reflected more than the oil or air. When the permittivity increases the degree of reflected electrical field will also increase. In addition, the electrical field lines also tend to bend more around

the phantom as the permittivity of the phantom gets higher because of the increasing of dielectric material.

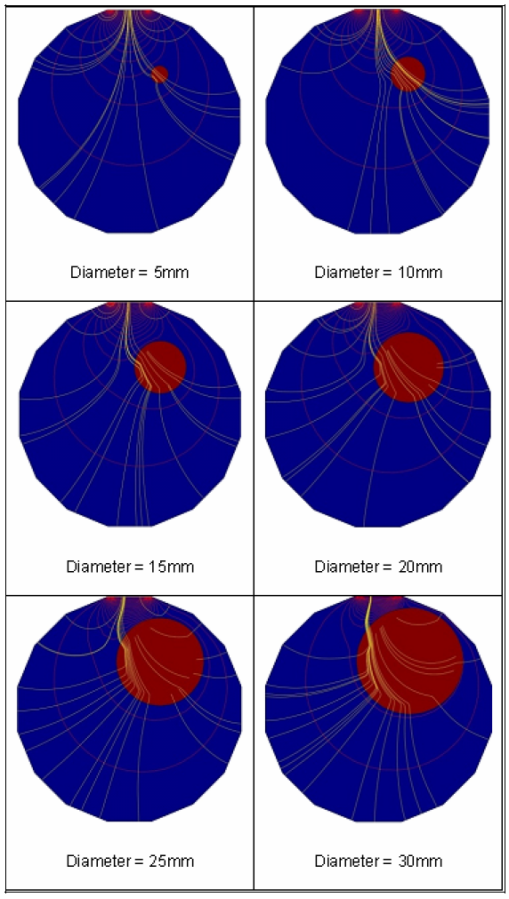

FIGURE 10. Electrical field lines with increasing of diameter of dielectric

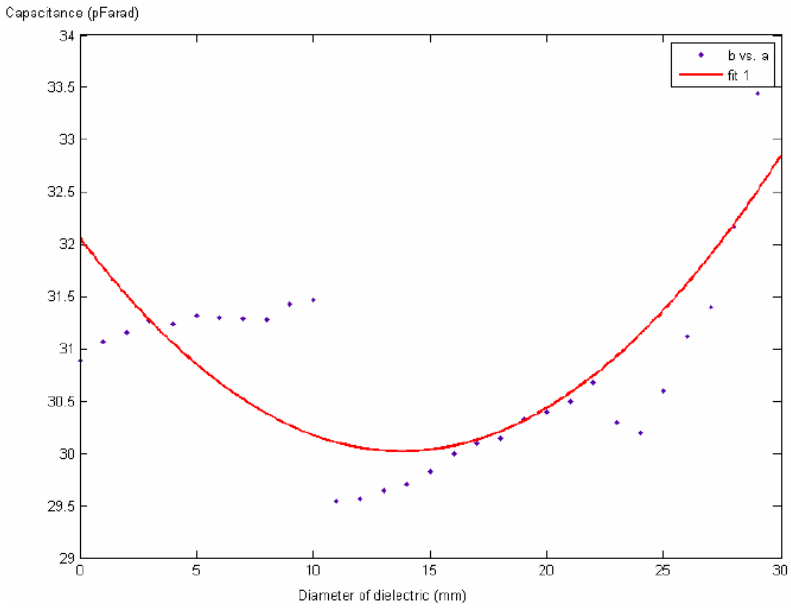

FIGURE 11. Model results for capacitance with increasing of diameter of dielectric

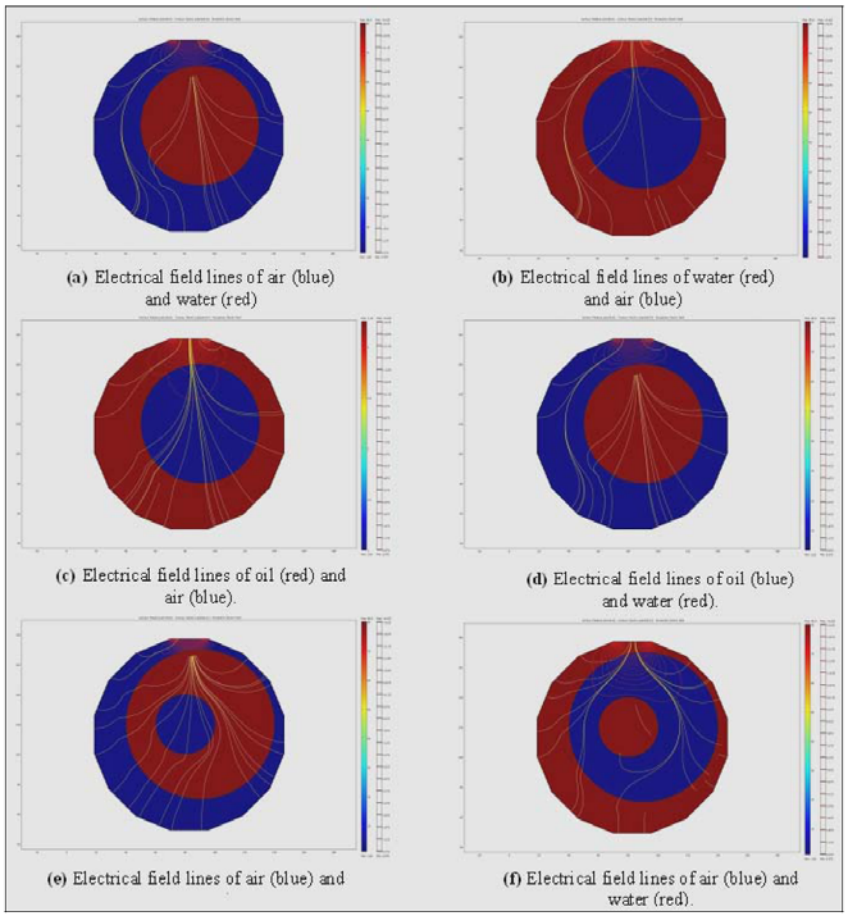

FIGURE 12. Degree of penetration of electrical field depends on the permittivity of the material (a)-(f)

7. **ECT Design Configuration.** In this research, 16 segmented electrodes have been fabricated onto the 110mm diameter pipeline. This sensor has been arranged symmetrically in hexadecagon surrounding the pipeline. It is very important that the pipeline material must be pure insulator to ensure that it has no effect on the measured signals. The placement of electrodes on the outer surface is done carefully to ensure that the electric field produced during the excitation is evenly distributed among the detecting electrodes. Due to this, the circle (cross-section) of the pipeline is divided equally into sixteen sectors, which each sector is 22.5°, as shown in Figure 13. The total width for one section is only 21.6mm.

7.1. **Sensor electrode design.** The portable ECT is developed by using special design PCB, as shown in Figure 14(a). Compare with the past design on ECT system, the new electrode sensor was no longer bended and sticked on the pipe wall. In this works, the electrodes are connected to the signal conditioning circuit directly without the cable to successfully eliminate most of the stray capacitance noise. This is very important because in ECT system it is very sensitive even to small noise such as from cable interfaces. Each electrode sensing has 19mm in width, and 100mm in length of the sensor area, copper and driven, the electrode length chosen was 10cm [13]. Several PCB sockets are soldered directly onto the bottom electrode plates, as illustrated in Figure 14(b). It is a necessary to rubdown the solder lead in order to make sure the sensing area is flat when it is sticked on the pipe wall.

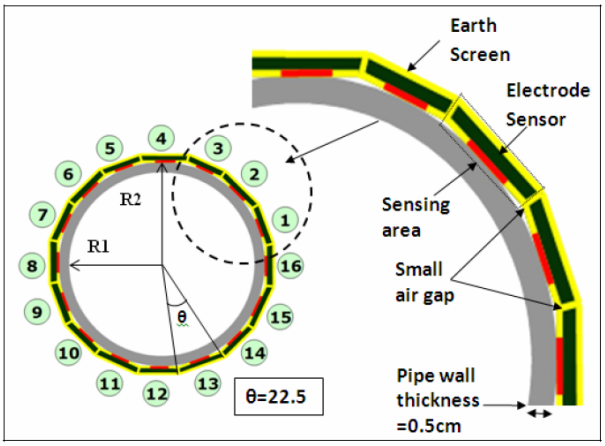

FIGURE 13. Cross sectional view of ECT sensor with 16 segmented portable electrodes

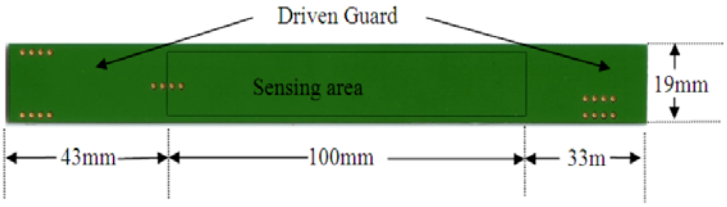

(a)

(b)

FIGURE 14. (a) Top of view electrode plate, (b) PCB sockets mounted onto bottom electrode plate

Next, the electrode will be directly connected to the measuring or signal conditioning circuit with male part connectors, as shown in Figure 15(a). The electrodes sensor is designed in a way that it can be plugged directly onto the PCB sockets of the signal conditioning circuit and becomes a single sensing module. Each of the electrodes is connected to a signal conditioning circuit via 1.0mm pitch PCB connectors as shown in Figure 15(b).

7.2. **Sensor measurement module.** Each of the measurement module is unique, and able to work independently because all the measuring operations are controlled by a single microcontroller on the circuit, and each of the circuits consists of; signal switching circuit, signal detection and amplifier circuit, absolute value circuit, low pass filter circuit, programmable gain amplifier (PGA), analog to digital converter circuit and a microcontroller control unit as shown in Figure 16. The desired sequence operation of electrode's signal selection, measuring data and conversion data is depended on programming in the microcontroller. Figure 17 shows the complete module of Portable ECT.

8. **Experimental Verification.** Experiments are performed using the test of 16-segmented ECT sensor electrodes to verify simulation illustrated in Figure 10. An annular water/air flow phantom was created in the ECT experiments using a few sizes of bottle and test tube also illustrated in Figure 18. This was achieved by inserting the bottle and test

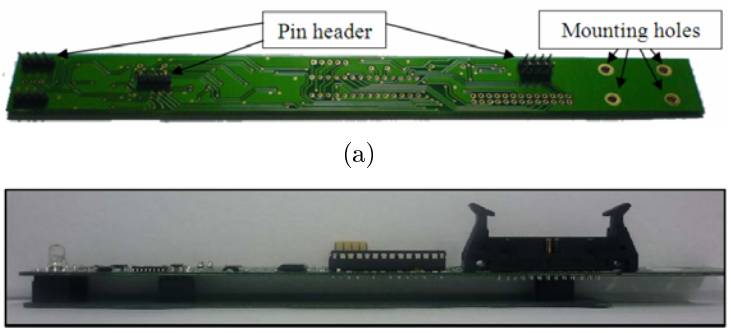

FIGURE 15. (a) The signal conditioning circuit with pin connectors, (b) electrode sensor module

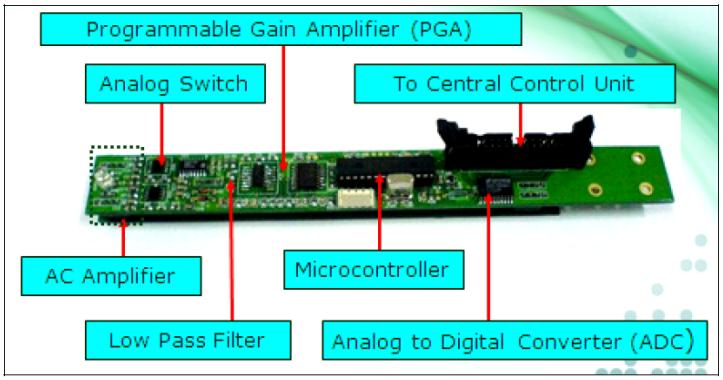

FIGURE 16. The ECT measurement module

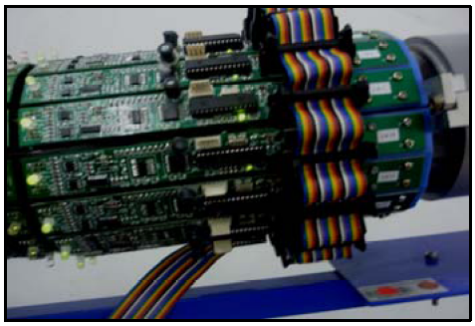

FIGURE 17. Complete portable ECT sensing module

tube inside the ECT sensor, and then filled up the bottle and test tube with water, and leaving the space between the inner ECT sensor wall and the outer bottle or test tube wall with air. The water used in the ECT experiments is tap water with relative permittivity, $\varepsilon_r = 80$.

8.1. **Linear relationship between the permittivity distribution and capacitance.** Inter-electrode capacitance value is measured using Digital Capacitance Meter by *GLK INSTRUMENTS* as shown in Figure 19. These types of digital capacitance meter provide analog outputs of the meter reading and of the reference voltage for radiometric measurements. These outputs can be connected to digital voltmeters, plotters, data loggers and computer data acquisition systems. The measured value of inter-electrode capacitance by

FIGURE 18. Portable ECT with bottle and test tube used to create phantoms inside the ECT sensor. Water is filled in the bottle and test tube, making up phantom of annular water flow.

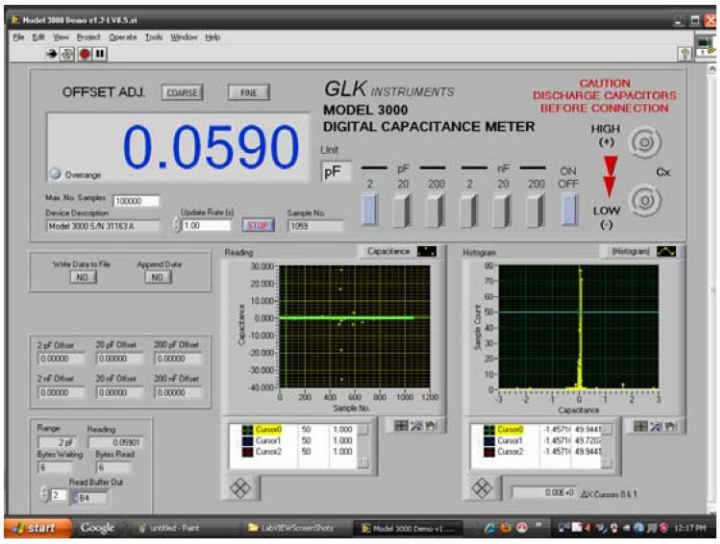

FIGURE 19. Digital capacitance meter monitoring system by *GLK INSTRUMENTS*

TABLE 2. Standing capacitance (pF) due to difference size (mm) of dielectric

Size of dielectric material	**Capacitance (pF)**
20mm	0.0590
35mm	0.0648
40mm	0.0716
55mm	0.0877
65mm	0.0884
80mm	0.1232

experimental due to difference size of dielectric material can be seen in Table 2. Measurement result, inter-electrode capacitance due to increasing the size of permittivity of the dielectric material shows in Figure 20.

8.2. **Two phase flow visualization experimental analysis.** A pipeline with a diameter of 110mm and pipe wall thickness of 6mm was used for two phase flow measurement

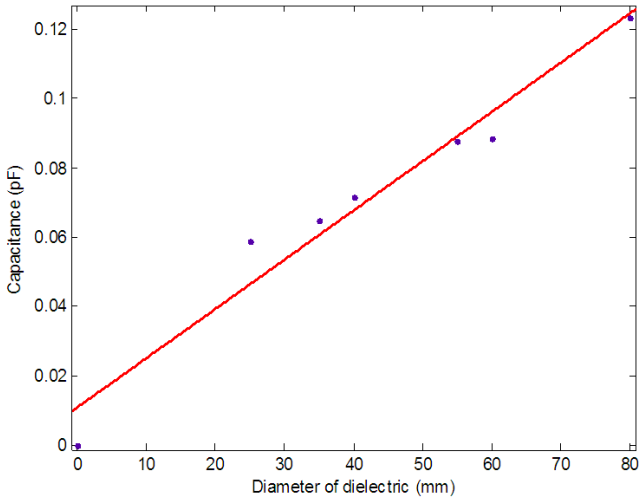

FIGURE 20. Inter-electrode capacitances measured value due to increasing the size of permittivity of the dielectric material, $\varepsilon_r = 80$

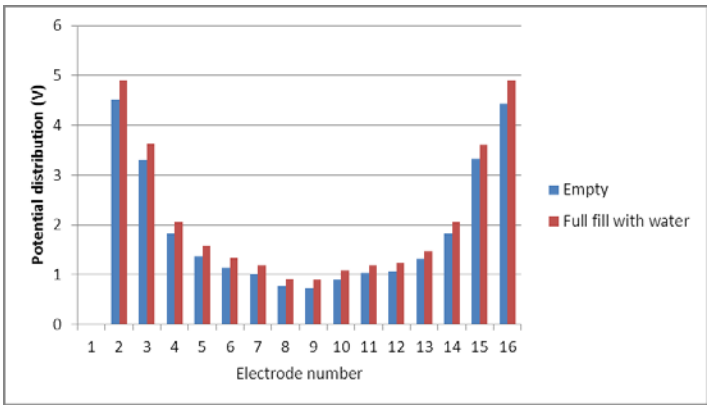

FIGURE 21. Data comparison between low-permittivity and high-permittivity in pipeline

experiments, water and gas. Figure 21 shows the potential distribution change if different permittivity filled inside pipeline.

Based on the output voltage, it can be seen that the highest value of the voltage happens at pair 1-2 and 1-16 for the first channel. This tells that adjacent pair of electrode will cause a high standing capacitance. While the lowest value happens at the pair 1-9, as the distance pair is escalating the standing capacitance will be reduced. Based on electromagnetic theory, this scenario happens when, the nearest two conducting material with any dielectric material between them produce higher density of magnetic field, therefore generate higher standing capacitance. Even though, its shows that, the standing capacitance may change due to the material that fill inside the pipeline such as shown in Figure 22.

In the first part of the experiment, the concentration of water is varied from 60% to 70%. The resulting images, based on the linear back projection algorithm are shown in Figure 23(a) when operating the reconstruction program in real-time. The processing speed is 25 frames per second, which depends on the speed of computer processor. The tomogram color tone represents concentration of water in the pipe. Concentration of water varies from low (white) to high (black). The second experiment is done to measure

the concentration profile for mixture water and palm oil inside pipeline as shown in Figure 23(b).

9. **Conclusions.** The electrostatic equation solver was sufficient to find the capacitance using COMSOL Multiphysic. According to the simulation results of fan beam 16 electrodes, the electrical properties such as potential difference, electrical field lines, potential lines, capacitance in ECT, and permittivity of the dielectric can be verified. The 2D and 3D geometries of ECT sensors was successful reconstructed.

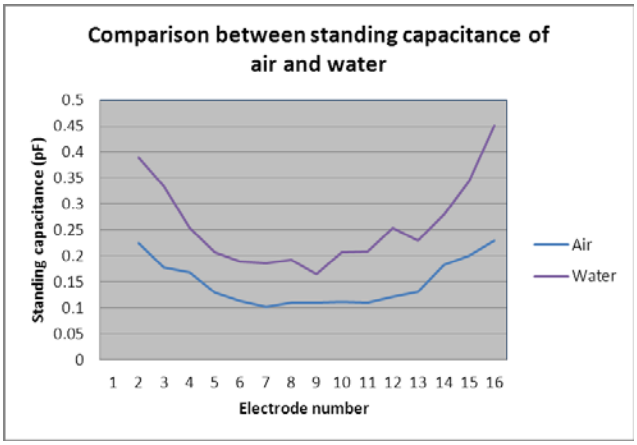

FIGURE 22. Comparison standing capacitance between air and water

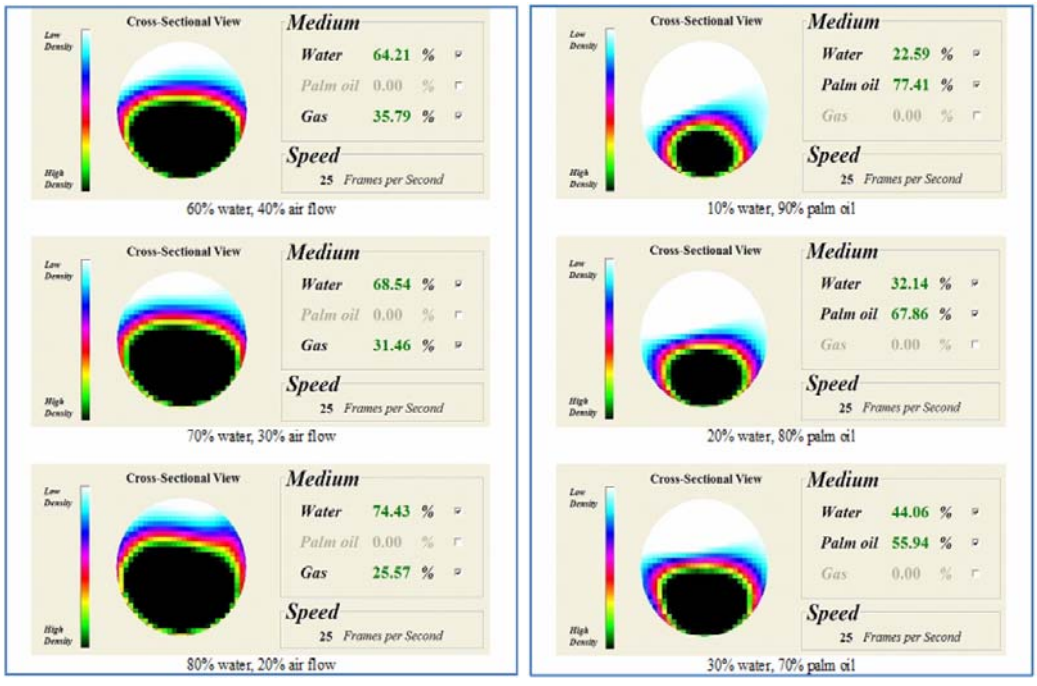

(a) (b)

FIGURE 23. Concentration profile for mixture (a) water/gas and (b) water/oil flow inside pipeline

The simulation and fabricating of the sensors electrodes, designing the segmented electrodes sensing circuit was successfully developed. The system is designed so that it becomes easier to direct mounting the signal conditioning PCB into electrode plate, which eliminates the cable noise.

Acknowledgment. This work was supported by Escience vot 79025 from Malaysian Government. Authors are grateful to the financial support by Research University Grant of Universiti Teknologi Malaysia (Grant No. Q.J130000.7123.00J04) and ScienceFund of Ministry of Science, Technology and Innovation, Malaysia (Grant No. 03-01-06-SF0193; Vot 79128).

REFERENCES

[1] M. Byar, Developments in electrical capacitance tomography, *PTL Application Notes*, 2001.

[2] Q. Marashdeh, W. Warsito, L.-S. Fan and F. L. Teixeira, A multimodal tomography system based on ECT sensors, *IEEE Sensors Journal*, vol.7, no.3, pp.426-433, 2007.

[3] T. Zhaoa, M. Takeia, K. Masakia, R. Ogisob, K. Nakaob and A. Uchiurac, Sensor design and image accuracy for application of capacitance CT to the petroleum refinery process, *Flow Measurement and Instrumentation Journal*, vol.18, pp.268-276, 2007.

[4] W. Q. Yang and L. Peng, Image reconstruction algorithms for electrical capacitance tomography, *Meas. Sci. Technol. Process Tomography Group, UMIST*, vol.14 / R1–R13, 2003.

[5] T. C. Tat, *Water/Oil Flowing Imaging of Electrical Capacitance Tomography System*, Bachelor Thesis, Universiti Teknologi Malaysia, 2003.

[6] W. Q. Yang, Design of electrical capacitance tomography sensors, *Meas. Sci. Technol. IOP*, vol.21, pp.233-957, 2010.

[7] E. J. Mohamad and R. A. Rahim, Multiphase flow reconstruction in oil pipelines by portable capacitance tomography, *Proc. of IEEE Sensors 2010 Conference*, HI, USA, pp.273-278, 2010.

[8] Z. Cao, L. Xu and H. Wang, Image reconstruction technique of electrical capacitance tomography for low-contrast dielectrics using Calderon's method, *Measurement Science and Technology*, vol.20, pp.104012-104027, 2009.

[9] Process Tomography Limited, Fundamental of ECT, *Electrical Capacitance Tomography System Operating Manual*, no.1, Cheshire, United Kingdom, 2009.

[10] H. Talib, J. M. Saleh and Z. A. Aziz, *Flow Process Identification from Electrical Capacitance Tomography Data Using Ensemble of Multilayer Perceptrons*, School of Electrical and Electronics Engineering Campus, Universiti Sains Malaysia, 2009.

[11] N. Flores, J. C. Gamio, C. Ortiz_Alemàn and E. Damiàn, Sensor modeling for an electrical capacitance tomograpgy system applied to oil industry, *Proc. of the COMSOL Multiphysocs User's Conference*, Boston, MA, USA, 2005.

[12] K. J. Alme and S. Mylvaganam, Analyzing 3D and conductivity effects in electrical tomography system using COMSOL multiphysics EM module, *Proc. of the Nordic COMSOL Conference*, 2006.

[13] D. Yang, B. Zhou, C. Xu, G. Tang and S. Wang, Effect of pipeline thickness on electrical capacitance tomography, *Journal of Physics: Conference Series*, vol.147, 2009.

[14] C. Zhou, X. Wei, Q. Zhang and B. Xiao, Image reconstruction for face recognition based on fast ICA, *International Journal of Innovative Computing, Information and Control*, vol.4, no.7, pp.1723-1732, 2008.

[15] J. Pan, C. Zhang and Q. Guo, Image enhancement based on the shearlet transform, *ICIC Express Letters*, vol.3, no.3(B), pp.621-626, 2009.

[16] Y. Zhang, C. Zhang, J. Chi and R. Zhang, An algorithm for enlarged image enhancement, *ICIC Express Letters*, vol.3, no.3(B), pp.669-674, 2009.